Enhanced Spin–Orbit Torques in Graphene by Pt Adatoms Decoration

Yifei Wang(王怡飞), Qi Zhang(张其), Haiming Xu(徐海茗), Xi Guo(郭玺), Yuhan Chang(常宇晗), Jianrong Zhang(张健荣), Xiaodong He(和孝东), Yalu Zuo(左亚路)*, Baoshan Cui(崔宝山)*, and Li Xi(席力)

Key Laboratory for Magnetism and Magnetic Materials of Ministry of Education, Lanzhou University, Lanzhou 730000, China

(Received 21 January 2024; accepted manuscript online 10 May 2024)

Graphene (Gr) with widely acclaimed characteristics, such as exceptionally long spin diffusion length at room temperature, provides an outstanding platform for spintronics. However, its inherent weak spin–orbit coupling (SOC) has limited its efficiency for generating the spin currents in order to control the magnetization switching process for applications in spintronics memories. Following the theoretical prediction on the enhancement of SOC in Gr by heavy atoms adsorption, here we experimentally observe a sizeable spin–orbit torques (SOTs) in Gr by the decoration of its surface with Pt adatoms in Gr/Pt($t_{\rm Pt}$)/FeNi trilayers with the optimal damping-like SOT efficiency around 0.55 by 0.6-nm-thick Pt layer adsorption. The value is nearly four times larger than that of the Pt/FeNi sample without Gr and nearly twice the value of the Gr/FeNi sample without Pt adsorption. The efficiency of the enhanced SOT in Gr by Pt adatoms is also demonstrated by the field-free SOT magnetization switching process with a relatively low critical current density around 5.4 MA/cm^2 in Gr/Pt/FeNi trilayers with the in-plane magnetic anisotropy. These findings pave the way for Gr spintronics applications, offering solutions for future low power consumption memories.

DOI: 10.1088/0256-307X/41/6/067502

Today, massive amounts of information place increasing demands on information processing and storage technology. In contrast to traditional semiconductor random-access memory, the magnetic random-access memory (MRAM) has been gaining more attention due to its non-volatility, high density, and low power consumption.[1–3] Among MRAMs, spin-orbit-torques (SOTs) driven MRAM has garnered significant attention with the merit on energy consumption and the separation of reading and writing paths compared to the former spin-transfer-torque MRAMs.[4–8] Usually, the efficient writing force comes from the spin current generated SOT in the heavy metal/ferromagnet bilayers via the spin Hall effect[5] and/or the interfacial Rashba effect.[4] The stronger the spin–orbit coupling (SOC) of materials is, the higher the generating efficiency of spin current from the charge current will be. Among lots of spin current generating materials,[9] including heavy metals, topological insulators, two-dimensional (2D) materials, etc., 2D materials[10–12] due to their unique spin-related properties, such as ultralong spin relaxation times and spin diffusion lengths, have brought new prospects for applications in spintronics, holding the potential for breakthroughs in low-power consumption, high storage density, and so on.

Graphene (Gr) as one of the 2D materials is particularly remarkable due to its widely acclaimed characteristics.[12,13] At room temperature, Gr exhibits exceptionally long spin diffusion lengths and effective spin-transport properties,[13–16] granting it significant advantages in long-distance spin propagation and manipulation. Additionally, the distinctive Dirac cone band structure of Gr offers potential performance advantages in reducing power consumption and enhancing the operational speed of storage units.[8] However, the weak SOC of Gr limits its ability for generating spin currents.[13,17] To observe spin-orbit effects in Gr, it seems necessary to enhance the SOC, without destroying the Dirac cone structure. In order to address this issue, various approaches have been explored, such as weakly hydrogenated Gr,[18] proximity effect in Gr,[19] and adsorption with heavy atoms (e.g., Au and Pt).[20–26] For instance, Abdelouahed *et al.* theoretically predicted that heavy atom (Au) adsorption could enhance SOC in Gr.[20] The reasons can be attributed to the hybridization between the 5*d* states of Au and the π states of Gr, leading to an enhanced spin–orbit splitting of the Gr π state, thereby increasing the SOC of Gr.[21,22,26] Theoretical calculation by Marchenko *et al.* predicted that this enhanced spin–orbit splitting is caused by the location of the heavy metal atoms in the hollow sites of Gr, while heavy metal atoms at other positions have minimal impact on the spin–orbit splitting.[21] However, Brey also find that the SOC enhancement effect can still be observed when adatoms are randomly distributed on the Gr surface,[27] as shown in Fig. 1(a). Therefore, we attribute the enhanced SOC of Pt atoms adsorbed on Gr surfaces to the collective effect of Pt atoms adhering across the entire Gr surface, rather than the contribution solely from specific locations of adsorption. Although the above-mentioned effective method to enhance the SOC of Gr was proved, the efficiency of spin current generation from adatoms modified Gr is rarely reported.[9,13,28]

In this work, we systematically investigate the rela-

*Corresponding authors. Email: zuoyl@lzu.edu.cn; cuibs@lzu.edu.cn
© 2024 Chinese Physical Society and IOP Publishing Ltd

tionship between SOT and the size of Pt atomic clusters adsorbed on the Gr surface in Gr/Pt(t_{Pt})/FeNi by the harmonic Hall measurement method. The results indicate that the SOT efficiency of Gr is significantly enhanced by adsorption of Pt atomic clusters onto Gr. Crucially, when $t_{Pt} = 0.6$ nm, the maximum value of effective spin Hall angle reaches 0.55, which is nearly four times larger than that of the Pt/FeNi sample without Gr and nearly twice the value of the Gr/FeNi sample without Pt adsorption. In addition, we also conduct magnetization switching tests on the Gr/Pt(0.6)/FeNi sample, achieving SOT-induced field-free magnetization switching at a relatively low critical current density level of 5.4 MA/cm^2. These research findings provide strong support and guidance for practical application of Gr in the field of spintronics, particularly in advancing the capabilities of SOT MRAMs.

At room temperature, Gr/Pt(t_{Pt})/FeNi(5) (thickness in nm) was deposited on a monolayer CVD-grown graphene film (Six Carbon Technology company) through direct current magnetron sputtering, with $t_{Pt} = 0$, 0.2, 0.4, 0.6, 0.8, and 1.0 nm. Additionally, a glass-substrate/Pt(0.6)/FeNi(5) reference sample was prepared by using the same method. To prevent the oxidation of the FeNi layer, a protective Ti layer of 3 nm was grown on all samples.

To demonstrate the quality of Gr after Pt growth, we conducted Raman spectroscopy tests on Gr/Pt(t_{Pt})/FeNi(5) samples. As depicted in Fig. 1(b), the significant features in the Raman spectrum of monolayer Gr include the G band at approximately 1586 cm^{-1} and the 2D band at around 2645 cm^{-1} using 633 nm laser excitation. Furthermore, the 2D band is characterized by a well-symmetric Lorentzian peak with a full width at half maximum of 27 cm^{-1}, confirming the high quality of Gr.[29] After the deposition of Pt layers, the G and 2D peaks of Gr remain intact, and Gr/Pt(t_{Pt})/FeNi(5) samples' ($t_{Pt} \neq 0$) Raman signals are significantly enhanced due to the surface-enhanced Raman scattering[30–33] employing 532 nm laser excitation [Gr/Pt(0.6)/FeNi(5) sample as an example]. It is worth mentioning that the position of 2D peak will shift with the change of excitation energy due to the double resonance process.[34] Furthermore, comparing with the Raman spectrum of pristine Gr, a distinct D band is clearly observed at 1345 cm^{-1}, attributed to the artificial defects induced by Pt adatoms on the Gr surface, whereas such defects do not change the properties of Gr.[31]

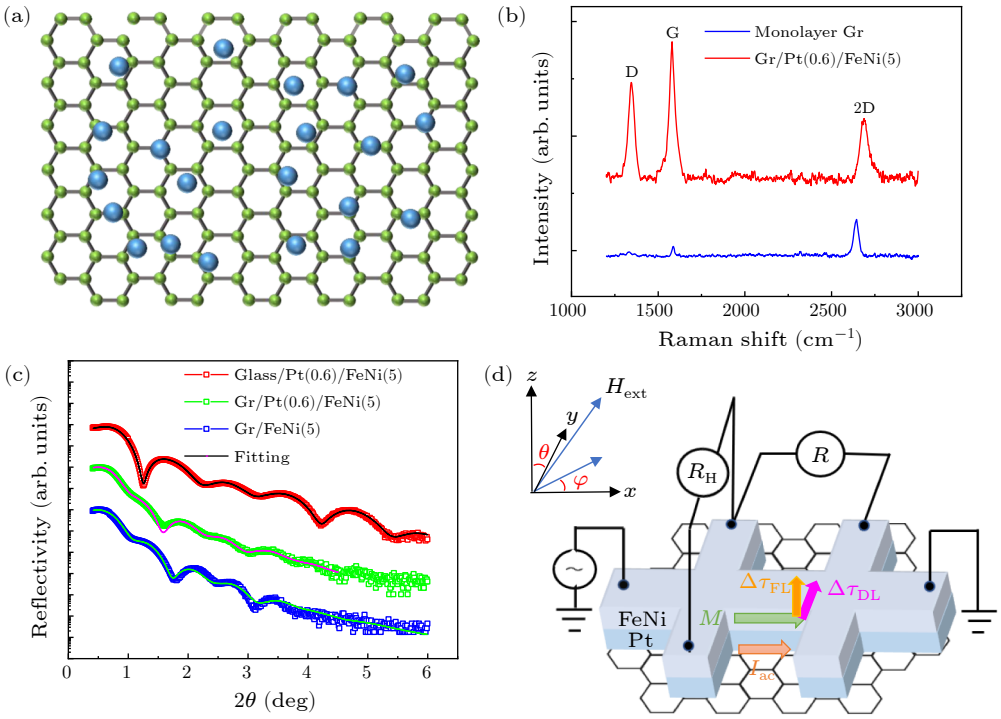

Fig. 1. (a) Heavy metal atoms are randomly distributed on the surface of Gr. (b) The Raman spectrum of monolayer pristine Gr excited by a 633 nm laser (blue solid line) and the surface-enhanced Raman scattering of Gr/Pt(0.6)/FeNi(5) samples excited by a 532 nm laser (red solid line). (c) XRR plots for Gr/FeNi(5), Gr/Pt(0.6)/FeNi(5), and glass/Pt(0.6)/FeNi(5). (d) Schematic Hall bars used for harmonic Hall resistance measurements.

The roughness/diffusion degree between layers and the thickness of each layer in Gr/Pt(t_{Pt})/FeNi(5) samples were characterized by the x-ray reflectivity (XRR). Figure 1(c) displays the XRR results of three representative samples. Based on the fitting results from the GenX software,[35,36] the actual structures of these three samples are determined to be: glass/Pt(1.0)/FeNi(4.8), Gr/FeNi(5.8), and Gr/Pt(0.5)/FeNi(5.8). The actual thicknesses of the samples are very close to the designed nominal thicknesses. The roughness distribution of each layer in each sample falls within the range of 0.2 nm–1.1 nm. It is worth noting that the interface with the maximum roughness comes

from the Pt/FeNi layer, indicating that the thinner Pt layer we grew is not continuous. It should be noted that, by comparing the XRR curves of three samples, it was observed that the sample on glass has more oscillation periods, indicating that the crystallinity of Pt(0.6)/FeNi(5) sample grown on glass is superior to those on Gr. The reason may be due to the lower roughness of glass compared to Gr, or Pt atoms are more prone to cluster formation on the Gr surface.

The deposited films were patterned into Hall-bar devices with size of 20 μm × 190 μm using the standard photolithography and Ar-ion milling techniques for all samples. The configuration for transport measurements is shown in Fig. 1(d) (for clarity, Pt deposited on Gr is represented as a layered structure), where θ and φ represent the polar and azimuthal angles of the external magnetic field ($H_{\rm ext}$), respectively. In the harmonic Hall resistance measurements, an alternating current with a frequency of 133 Hz was applied in the x-axis direction, and the Hall resistance signal was collected in the y-axis direction through a high-precision data acquisition card (NI-4461).[37] Then, the Hall resistance signal is separated by fast Fourier transform to the harmonic signals, ultimately the first harmonic Hall resistance ($R_{1\omega}$) and second harmonic Hall resistance ($R_{2\omega}$) were obtained. The injection of an alternating current $I_{\rm ac}$ generates two distinct types of SOTs: field-like (FL) torque, $\sim \boldsymbol{m} \times \hat{\boldsymbol{y}}$, and damping-like (DL) torque, $\sim \boldsymbol{m} \times (\boldsymbol{m} \times \hat{\boldsymbol{y}})$, where $\boldsymbol{m}$ is the magnetization unit vector, and $\hat{\boldsymbol{y}}$ is the unit vector, representing the direction of accumulated spins at the interface.[38,39] All measurements were performed at room temperature.

We independently quantified the effective field of the DL ($H_{\rm DL}$) and FL ($H_{\rm FL}$) torques for each sample using the harmonic Hall resistance measurements method. The SOT generated from the applied alternating current will cause the magnetic moments of the ferromagnetic layer to oscillate around their equilibrium positions. This microscopic behavior manifests as small-angle vibrations, ultimately resulting in changes in the Hall resistance.[40] Each harmonic Hall resistance can be expressed (when applying an $H_{\rm ext}$ in the x–y plane, i.e., $\theta = 90°$) as follows:[40,41]

$$R_{1\omega} = R_{\rm PHE}\sin(2\varphi), \tag{1}$$

$$\begin{aligned} R_{2\omega} &= \left(\frac{1}{2}R_{\rm AHE}\frac{H_{\rm DL}}{H_{\rm K}+H_{\rm ext}} + R_{\nabla T_z}\right)\cos\varphi \\ &\quad - R_{\rm PHE}\frac{H_{\rm FL}+H_{\rm Oe}}{H_{\rm ext}}\cos\varphi\cos(2\varphi) + R_{\nabla T_x}\sin(2\varphi), \\ &\equiv R_{{\rm DL}+\nabla T_z}\cos\varphi + R_{{\rm FL}+{\rm Oe}}\cos\varphi\cos(2\varphi) \\ &\quad + R_{\nabla T_x}\sin(2\varphi). \end{aligned} \tag{2}$$

Here, $R_{\rm PHE}$, $R_{\rm AHE}$, $H_{\rm K}$, and $H_{\rm Oe}$ correspond to the plane Hall resistance, anomalous Hall resistance, out-of-plane anisotropic field, and current-induced Oersted field, respectively. $R_{\nabla T_z}$ and $R_{\nabla T_x}$ are the thermal-induced second harmonic resistance generated by anomalous Nernst signals from the perpendicular thermal gradient (∇T_z) and planar Nernst signals associated with the longitudinal temperature gradient (∇T_x), respectively. It should be mentioned that the $R_{\nabla T_x}$ does not depend on $H_{\rm ext}$.[42] Due to the same symmetry of $H_{\rm DL}$ and the ∇T_z induced contributions, they appear in pairs in Eq. (2).[43] The contributions of $H_{\rm FL}$ and $H_{\rm Oe}$ also have the same symmetry. As shown in Eq. (2), we define the coefficients of the $\cos\varphi$ and $\cos\varphi\cos(2\varphi)$ components in Eq. (2) as $R_{{\rm DL}+\nabla T_z}$ and $R_{{\rm FL}+{\rm Oe}}$, respectively, which can be separated by fitting $R_{2\omega}$ with φ.[43]

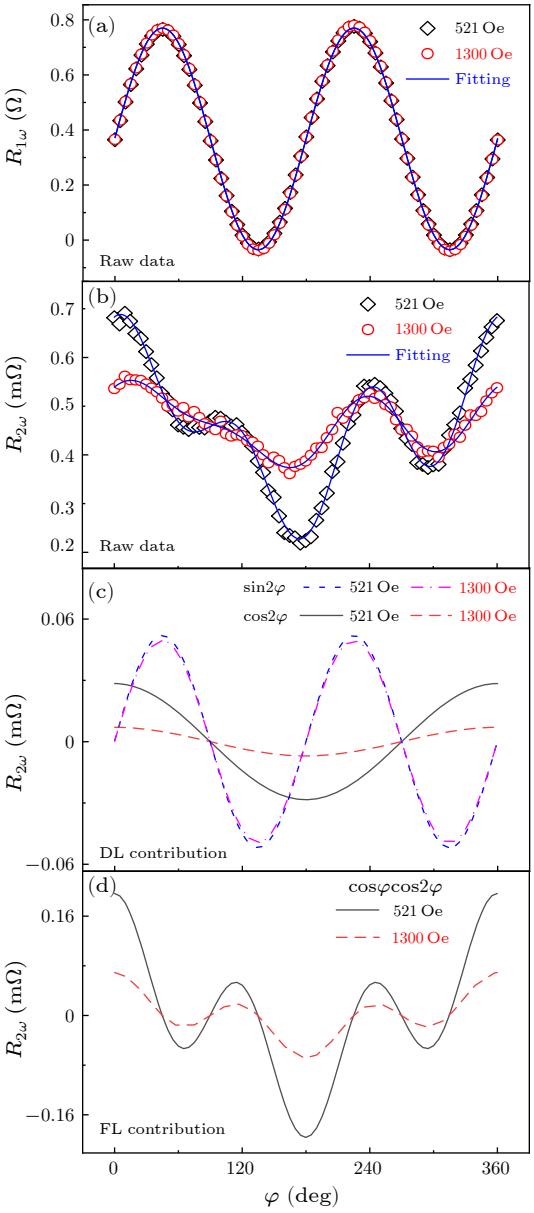

Fig. 2. (a) The raw data of $R_{1\omega}$ measured at 521 Oe (black open diamond) and 1300 Oe (red open circle) for the Gr/Pt(0.6)/FeNi(5) sample. The solid blue line is the fit result with Eq. (1). (b) The raw data of $R_{2\omega}$. The solid blue line is the fit result with Eq. (2). (c) The DL contribution $\cos\varphi$ component and antisymmetric $\sin(2\varphi)$ signals separated from $R_{2\omega}$. (d) The FL contribution $\cos\varphi\cos(2\varphi)$ component extracted from $R_{2\omega}$.

Figure 2(a) shows the variation of $R_{1\omega}$ concerning φ for Gr/Pt(0.6)/FeNi(5) when the applied magnetic fields are $H_{\rm ext}$ = 521 Oe and 1300 Oe. It can be observed that the trend of $R_{1\omega}$ for φ is consistent with Eq. (1). Moreover, its amplitude does not change with $H_{\rm ext}$, indicating that the magnetization has been fully saturated.[43] By fitting the φ dependence of $R_{1\omega}$ via Eq. (1) [as shown by the blue line in Fig. 2(a)], $R_{\rm PHE}$ can be obtained. Figure 2(b) dis-

plays the raw data of $R_{2\omega}$. It is worth noting that the $R_{2\omega}$ measured in our sample differs slightly from the conventional symmetric signal around 180°.[41,43] It contains an additional antisymmetric signal with an angle dependence of $\sin(2\varphi)$, as described in Eq. (2). Regarding the source of the antisymmetric $\sin(2\varphi)$ signal, it has been reported in the literature that it may come from a planar Nernst signal induced by the ∇T_x within the sample.[42] The solid blue line in Fig. 2(b) represents the fitting results by Eq. (2). According to Eq. (2), the DL- and FL-SOTs generated by the spin current can be separated based on the different angle dependencies, corresponding to Figs. 2(c) and 2(d), respectively. With increasing $H_{\rm ext}$, the coefficients $R_{\rm DL+\nabla T_z}$ and $R_{\rm FL+Oe}$ containing SOT-generated DL and FL contribution to $R_{2\omega}$ will both decrease. The antisymmetric $\sin(2\varphi)$ signal is also extracted, as shown in Fig. 2(c), and it does not change with $H_{\rm ext}$.[42]

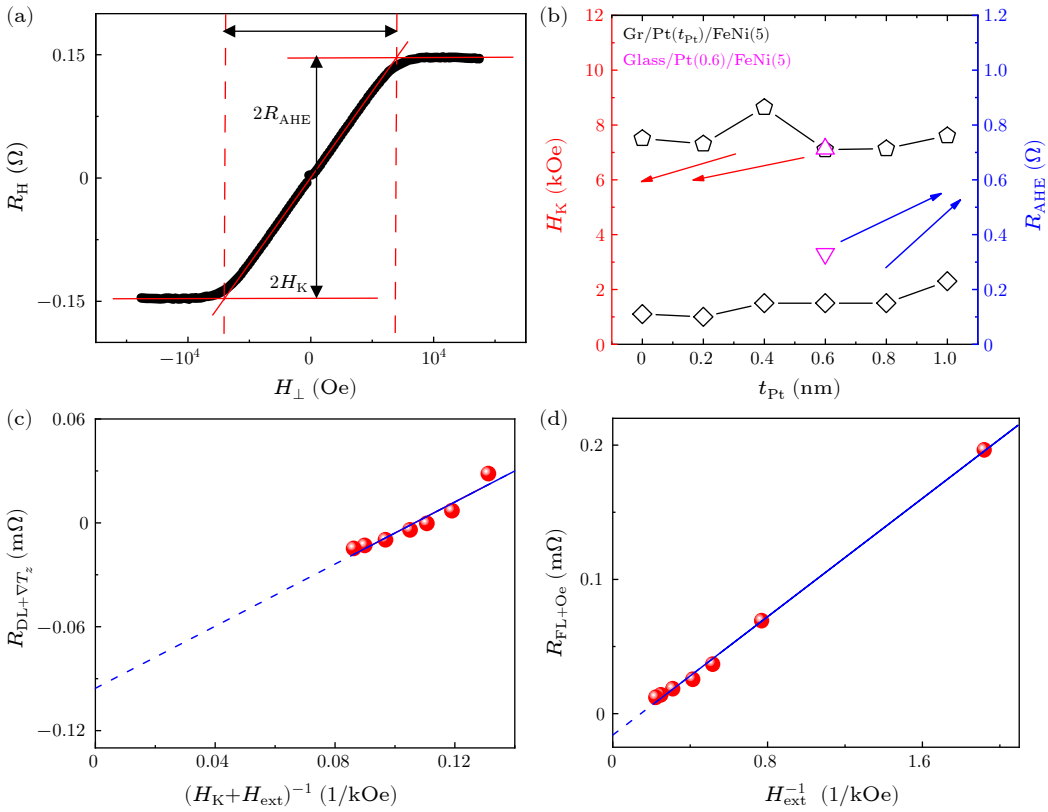

Fig. 3. (a) The anomalous Hall resistance loop of Gr/Pt(0.6)/FeNi(5). $R_{\rm AHE}$ and $H_{\rm K}$ obtained are marked in the figure. (b) $H_{\rm K}$ and $R_{\rm AHE}$ as functions of Pt thickness, along with the corresponding values for the glass/Pt(0.6)/FeNi(5). (c) $R_{\rm DL+\nabla T_z}$ as a function of $(H_{\rm K}+H_{\rm ext})^{-1}$ in the Gr/Pt(0.6)/FeNi(5) sample. (d) $R_{\rm FL+Oe}$ as a function of $H_{\rm ext}^{-1}$. The solid blue line represents the result of the linear fitting of the data.

To evaluate the influence of Pt adatoms on the SOT in Gr/Pt($t_{\rm Pt}$)/FeNi(5), we extract $H_{\rm DL}$ and $H_{\rm FL}$ of SOTs. $H_{\rm DL}$ and $H_{\rm FL}$ can be obtained from the coefficient of the value of $R_{\rm DL+\nabla T_z}$ and $R_{\rm FL+Oe}$, respectively, according to Eq. (2), where $R_{\rm PHE}$, $R_{\rm AHE}$, and $H_{\rm K}$ are parameters. $R_{\rm PHE}$ has been obtained by fitting $R_{1\omega}$ using Eq. (1). $R_{\rm AHE}$ and $H_{\rm K}$ are obtained from the anomalous Hall resistance loops by applying $H_\perp$ along the z-axis ($\theta = 0°$), as shown in Fig. 3(a) for the exemplary Gr/Pt(0.6)/FeNi(5) sample.

The $R_{\rm AHE}$ and $H_{\rm K}$ values for the Gr/Pt($t_{\rm Pt}$)/FeNi(5) and Pt(0.6)/FeNi(5) reference samples are summarized in Fig. 3(b). $R_{\rm AHE}$ and $H_{\rm K}$ are basically independent of the sample and thus do not affect the analysis of harmonic Hall resistance. Figure 3(c) shows the $R_{\rm DL+\nabla T_z}$ obtained by separating the DL contributions for the Gr/Pt(0.6)/FeNi(5) sample. It is linearly related to $(H_{\rm K}+H_{\rm ext})^{-1}$, which reflects the suppression of the DL contribution at large external field. The slope gives the DL-SOT effective field $H_{\rm DL}$. The intercept represents the thermal contribution caused by anomalous Nernst effect[44] and/or the spin Seebeck effect.[45] Similarly, by linearly fitting the data in Fig. 3(d) (note that this data does not pass through the origin completely, and the small residual offset depends on the accuracy of the magnetization angle and possible unintentional misalignment of $H_{\rm ext}$ relative to the x–y plane),[41] we can obtain the FL-SOT effective fields $H_{\rm FL}$ and $H_{\rm Oe}$. According to the simplified Ampere's law,[43] by subtracting the contribution of $H_{\rm Oe}$ through $I_{\rm Pt}/2w$, where $I_{\rm Pt}$ is the charge current flowing in the Pt and Gr layers, and w the width of the Hall-bar, we can obtain $H_{\rm FL}$.

Figures 4(a) and 4(b) show the DL- and FL-SOTs effective field per current density J as a function of Pt thickness, respectively. Notably, Gr/FeNi exhibits a relatively large DL-SOT efficiency from charge current to

spin current, potentially attributed to Gr itself becoming a source of spin-polarized electrons due to proximity-induced spin splitting.[46] Subsequently, by comparing the DL-SOT efficiencies of Gr/Pt(t_{Pt})/FeNi, Gr/FeNi, and glass/Pt(0.6)/FeNi, the DL-SOT efficiency in the Gr/Pt(t_{Pt})/FeNi system is significantly higher, indicating that the Pt atomic adsorption on Gr further enhances the SOT effect. We believe that this enhanced effect results from the synergistic action of Gr/Pt. To obtain the ability of Gr by Pt adatoms from charge current to spin current, we evaluate the effective spin Hall angle (θ) with DL and FL characteristics based on the following equations:[47,48]

$$\theta_{DL(FL)} = \frac{2eM_S t_{FeNi}}{\hbar}\frac{H_{DL(FL)}}{J}, \tag{3}$$

where e, M_S, t_{FeNi}, and $\hbar$ represent the elementary charge, saturation magnetization, ferromagnet thickness, and Planck constant, respectively. Based on this formula and the above experimental results, θ_{DL} and θ_{FL} for Gr/Pt(t_{Pt})/FeNi(5) samples with different Pt thickness were obtained, as shown in Figs. 4(c) and 4(d). We can see that the θ_{DL} increases first and then decreases with the thickness of Pt. This is due to the fact that, while modifying Gr with heavy metal atomic adsorption can increase its SOC, higher coverage of these adsorbed atoms on Gr triggers various corresponding parasitic phenomena.[49] Yet, these phenomena do not dominate for a small number of randomly positioned heavy metal atoms.[49] When $t_{Pt} = 0.6$ nm, the maximum value is $\theta_{DL} = 0.55$, which is nearly four times larger than that of the Pt(0.6)/FeNi(5) sample without Gr and nearly twice the value of the Gr/FeNi(5) sample without Pt adsorption ($\theta_{DL} = 0.31$). This indicates that Gr modified by the Pt atomic clusters exhibits a strong SOC, leading to a considerably large SOT efficiency. Moreover, FL-SOT efficiency θ_{FL} ranges from 0.011 to 0.015, as shown in Fig. 4(d). These values are much smaller than those of the DL-SOT mentioned above. Therefore, we believe that FL-SOT is attributed to interface effects (such as Rashba–Edelstein effect), which exhibits thickness-independent behavior.[50,51] Notably, the magnitude of the H_{FL} signal in the Gr/FeNi sample is very small in order of μΩ, consequently, the fitting error and H_{FL} value have the same order of magnitude. Thus, the accurate value of θ_{FL} has not been shown in Fig. 4(d).

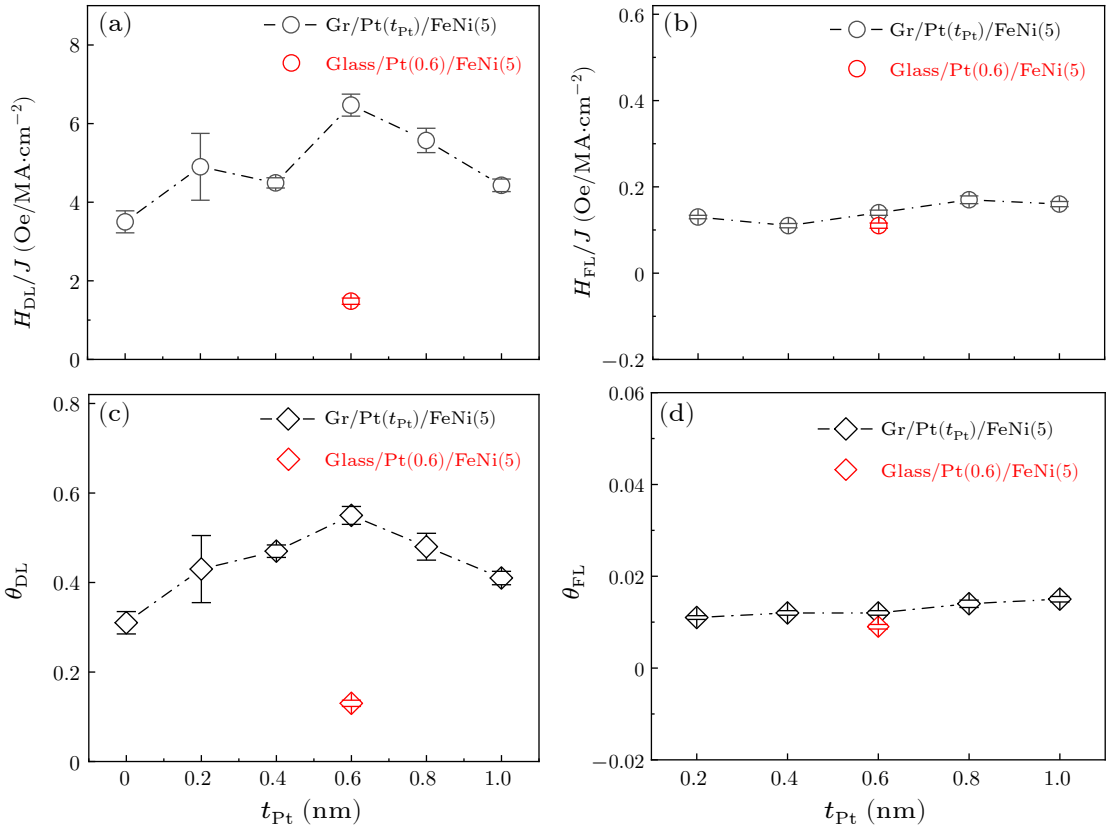

Fig. 4. (a) H_{DL}/J, (b) H_{FL}/J, (c) θ_{DL}, and (d) θ_{FL} versus Pt thickness, and the results for the corresponding glass/Pt(0.6)/FeNi(5).

To confirm the large efficiency from charge current to spin current of Pt adatoms decorated Gr, we conducted an independent magnetization switching measurement on the Gr/Pt(0.6)/FeNi(5) sample using the differential planar Hall effect (PHE) method. For the in-plane magnetized sample, the differential PHE method could allow one to clearly determine the direction of the magnetic moments in the ferromagnetic layer, either by magnetic field driven or by the SOT driven magnetization switching. In this method, we first applied a write magnetic field H_y along the y direction, i.e., the easy axis of the sample. H_y must be greater than the easy-axis coer-

civity to initialize the magnetization in a single domain state. Subsequently, H_y is removed, and then the read current $I_{\rm RD}$ and an excitation field $\pm H_x$ in the x direction are applied. Hall resistance values are measured under $\pm H_x$, and the differential PHE signal is obtained as $\Delta R_{\rm PHE} = (V_{+H_x} - V_{-H_x})/I_{\rm RD}$.[52] This sequence is then repeated for new values of H_y. Here, the magnitude of $\Delta R_{\rm PHE}$ is proportional to the size of H_x, which is used to rotate the magnetization through a small angle away from the y direction.

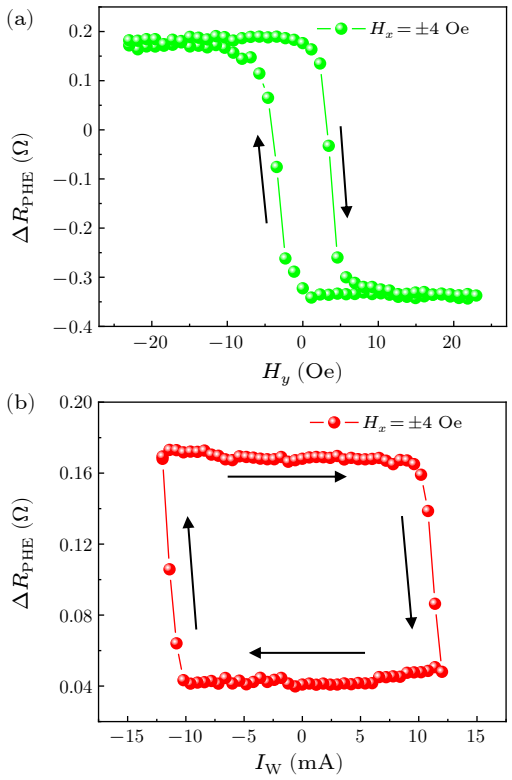

Fig. 5. Gr/Pt(0.6)/FeNi(5) (a) field and (b) current-induced switching curves.

Figure 5(a) shows the curves of the field-induced magnetization switching measured in this manner. One can determine that the switching field of the sample is approximately 3.6 Oe, which is consistent with the coercivity obtained from the hysteresis loops. Subsequently, a pulse current-induced magnetization switching is conducted. It is worth noting that because the magnetization direction is consistent with the internal spin polarization direction, no auxiliary magnetic field is required to achieve magnetization switching.[53] During the test process, a write pulse current $I_{\rm W}$ with pulse width around 1 ms is applied along the x direction, and the remaining steps are the same as before. Importantly, the magnetization switching can be achieved by pulse current generated SOT, as shown in Fig. 5(b). For the Gr/Pt(0.6)/FeNi(5) sample, the critical switching current $I_{\rm c} = 9.8$ mA corresponds to a critical switching current density $J_{\rm c} = 5.4\,{\rm MA/cm^2}$, which is close to our previous results in Pt/Co/Ta samples, in which the enhancement of SOT was achieved by select the heavy metals Pt and Ta with strong and different signs of spin Hall angles.[54] If the shunting effect is taken into account, the critical switching current density will be even smaller. The small switching ratio by SOT in our samples may be due to the shape anisotropy induced multidomain formation. It should be mentioned that the applied field H_x do not assist the magnetization switching whenever in the H_y-field-driven or in SOT-driven switching process. Moreover, the quite low critical switching current density independently suggests that the decoration of Pt adatoms on the surface of Gr could lower the energy consumption for Gr spintronics memories.

In summary, with the decoration of Pt on the surface of Gr, we have observed an enhanced spin current generating efficiency in Gr/Pt/FeNi trilayers with in-plane magnetic anisotropy by the harmonic Hall measurement method. In particular, when $t_{\rm Pt} = 0.6$ nm, the maximum value of effective spin Hall angle reaches 0.55, which is nearly four times larger than that of the Pt/FeNi sample without Gr and nearly twice the value of the Gr/FeNi sample without Pt adsorption. Furthermore, the field-free SOT magnetization switching can be achieved with a relatively low critical current density of $5.4\,{\rm MA/cm^2}$. These findings pave the way for Gr spintronics applications, offering solutions for future low power consumption memories.

Acknowledgments. This work was supported by the National Key R&D Program of China (Grant No. 2021YFB3501304), the National Natural Science Foundation of China (Grant Nos. 91963201 and 51671098), the 111 Project (Grant No. B20063), the Open Research Fund of Songshan Lake Materials Laboratory (Grant No. 2023SLABFN05), the Program for Changjiang Scholars and Innovative Research Team in University PCSIRT (Grant No. IRT16R35), the Fundamental Research Funds for the Central Universities (Grant No. lzujbky-2021-ct01), and the Natural Science Foundation of Gansu Province (Grant No. 22JR5RA474).

References

[1] Wolf S A, Awschalom D D, Buhrman R A, Daughton J M, von Molnár S, Roukes M L, Chtchelkanova A Y, and Treger D M 2001 *Science* **294** 1488

[2] Wolf S A, Lu J, Stan M R, Chen E, and Treger D M 2010 *Proc. IEEE* **98** 2155

[3] Ikegawa S, Mancoff F B, Janesky J, and Aggarwal S 2020 *IEEE Trans. Electron Devices* **67** 1407

[4] Miron I M, Garello K, Gaudin G, Zermatten P J, Costache M V, Auffret S, Bandiera S, Rodmacq B, Schuhl A, and Gambardella P 2011 *Nature* **476** 189

[5] Liu L, Pai C F, Li Y, Tseng H W, Ralph D C, and Buhrman R A 2012 *Science* **336** 555

[6] Cubukcu M, Boulle O, Drouard M, Garello K, Onur Avci C, Mihai Miron I, Langer J, Ocker B, Gambardella P, and Gaudin G 2014 *Appl. Phys. Lett.* **104** 042406

[7] Dieny B, Prejbeanu I L, Garello K, Gambardella P, Freitas P, Lehndorff R, Raberg W, Ebels U, Demokritov S O, Akerman J, Deac A, Pirro P, Adelmann C, Anane A, Chumak A V, Hirohata A, Mangin S, Valenzuela S O, OnbaşlıM C, d'Aquino M, Prenat G, Finocchio G, Lopez-Diaz L, Chantrell R, Chubykalo-Fesenko O, and Bortolotti P 2020 *Nat. Electron.* **3** 446

[8] Rybkina A A, Rybkin A G, Klimovskikh I I, Skirdkov P N, Zvezdin K A, Zvezdin A K, and Shikin A M 2020 *Nanotechnology* **31** 165201

[9] Song C, Zhang R, Liao L, Zhou Y, Zhou X, Chen R, You Y, Chen X, and Pan F 2021 *Prog. Mater. Sci.* **118** 100761

[10] Novoselov K S, Geim A K, Morozov S V, Jiang D, Zhang Y, Dubonos S V, Grigorieva I V, and Firsov A A 2004 *Science* **306** 666

[11] Wang Q H, Kalantar-Zadeh K, Kis A, Coleman J N, and Strano M S 2012 *Nat. Nanotechnol.* **7** 699

[12] Yang H, Valenzuela S O, Chshiev M, Couet S, Dieny B, Dlubak B, Fert A, Garello K, Jamet M, Jeong D E, Lee K, Lee T, Martin M B, Kar G S, Sénéor P, Shin H J, and Roche S 2022 *Nature* **606** 663

[13] Avsar A, Ochoa H, Guinea F, Özyilmaz B, van Wees B J, and Vera-Marun I J 2020 *Rev. Mod. Phys.* **92** 021003

[14] Barreiro A, Lazzeri M, Moser J, Mauri F, and Bachtold A 2009 *Phys. Rev. Lett.* **103** 076601

[15] Han W, Kawakami R K, Gmitra M, and Fabian J 2014 *Nat. Nanotechnol.* **9** 794

[16] Wen H, Dery H, Amamou W, Zhu T, Lin Z, Shi J, Žutić I, Krivorotov I, Sham L J, and Kawakami R K 2016 *Phys. Rev. Appl.* **5** 044003

[17] Castro Neto A H and Guinea F 2009 *Phys. Rev. Lett.* **103** 026804

[18] Balakrishnan J, Kok Wai Koon G, Jaiswal M, Castro Neto A H, and Özyilmaz B 2013 *Nat. Phys.* **9** 284

[19] Wang Z, Ki D K, Chen H, Berger H, MacDonald A H, and Morpurgo A F 2015 *Nat. Commun.* **6** 8339

[20] Abdelouahed S, Ernst A, Henk J, Maznichenko I V, and Mertig I 2010 *Phys. Rev. B* **82** 125424

[21] Marchenko D, Varykhalov A, Scholz M R, Bihlmayer G, Rashba E I, Rybkin A, Shikin A M, and Rader O 2012 *Nat. Commun.* **3** 1232

[22] Shikin A M, Rybkin A G, Marchenko D, Rybkina A A, Scholz M R, Rader O, and Varykhalov A 2013 *New J. Phys.* **15** 013016

[23] Balakrishnan J, Koon G K W, Avsar A, Ho Y, Lee J H, Jaiswal M, Baeck S J, Ahn J H, Ferreira A, Cazalilla M A, Castro Neto A H, and Özyilmaz B 2014 *Nat. Commun.* **5** 4748

[24] Calleja F, Ochoa H, Garnica M, Barja S, Navarro J J, Black A, Otrokov M M, Chulkov E V, Arnau A, Vázquez de Parga A L, Guinea F, and Miranda R 2014 *Nat. Phys.* **11** 43

[25] Klimovskikh I I, Tsirkin S S, Rybkin A G, Rybkina A A, Filianina M V, Zhizhin E V, Chulkov E V, and Shikin A M 2014 *Phys. Rev. B* **90** 235431

[26] Rybkin A G, Rybkina A A, Otrokov M M, Vilkov O Y, Klimovskikh I I, Petukhov A E, Filianina M V, Voroshnin V Y, Rusinov I P, Ernst A, Arnau A, Chulkov E V, and Shikin A M 2018 *Nano Lett.* **18** 1564

[27] Brey L 2015 *Phys. Rev. B* **92** 235444

[28] Ghising P, Biswas C, and Lee Y H 2023 *Adv. Mater.* **35** 2209137

[29] Casiraghi C, Pisana S, Novoselov K S, Geim A K, and Ferrari A C 2007 *Appl. Phys. Lett.* **91** 233108

[30] Schedin F, Lidorikis E, Lombardo A, Kravets V G, Geim A K, Grigorenko A N, Novoselov K S, and Ferrari A C 2010 *ACS Nano* **4** 5617

[31] Wang P, Zhang D, Zhang L, and Fang Y 2013 *Chem. Phys. Lett.* **556** 146

[32] Lee J, Shim S, Kim B, and Shin H S 2011 *Chem. Eur. J.* **17** 2381

[33] Zhan Z, Liu L, Wang W, Cao Z, Martinelli A, Wang E, Cao Y, Chen J, Yurgens A, and Sun J 2016 *Adv. Opt. Mater.* **4** 2021

[34] Ferrari A C, Meyer J C, Scardaci V, Casiraghi C, Lazzeri M, Mauri F, Piscanec S, Jiang D, Novoselov K S, Roth S, and Geim A K 2006 *Phys. Rev. Lett.* **97** 187401

[35] Björck M and Andersson G 2007 *J. Appl. Crystallogr.* **40** 1174

[36] Yun J, Sheng Y, Guo X, Zheng B, Chen P, Cao Y, Yan Z, He X, Jin P, Li J, Cui M, Shen T, Wang Z, Yang D, Zuo Y, and Xi L 2021 *Phys. Rev. B* **104** 134416

[37] Yun J, Bai Q, Yan Z, Chang M, Mao J, Zuo Y, Yang D, Xi L, and Xue D 2020 *Adv. Funct. Mater.* **30** 1909092

[38] Kim J, Sinha J, Hayashi M, Yamanouchi M, Fukami S, Suzuki T, Mitani S, and Ohno H 2013 *Nat. Mater.* **12** 240

[39] Garello K, Miron I M, Avci C O, Freimuth F, Mokrousov Y, Blügel S, Auffret S, Boulle O, Gaudin G, and Gambardella P 2013 *Nat. Nanotechnol.* **8** 587

[40] Wang W, Yan Z, Cao Y, Gao C, Shi Z, Si M, Cao J, Xi L, Yang D, and Xue D 2022 *Adv. Funct. Mater.* **32** 2204212

[41] Avci C O, Garello K, Gabureac M, Ghosh A, Fuhrer A, Alvarado S F, and Gambardella P 2014 *Phys. Rev. B* **90** 224427

[42] Liu Q, Lin X, and Zhu L 2023 *Adv. Sci.* **10** 2301409

[43] Ueda K, Moriuchi N, Fukushima K, Kida T, Hagiwara M, and Matsuno J 2020 *Phys. Rev. B* **102** 134432

[44] Bauer G E W, Saitoh E, and van Wees B J 2012 *Nat. Mater.* **11** 391

[45] Uchida K, Takahashi S, Harii K, Ieda J, Koshibae W, Ando K, Maekawa S, and Saitoh E 2008 *Nature* **455** 778

[46] Asshoff P U, Sambricio J L, Rooney A P, Slizovskiy S, Mishchenko A, Rakowski A M, Hill E W, Geim A K, Haigh S J, Fal'ko V I, Vera-Marun I J, and Grigorieva I V 2017 *2D Mater.* **4** 031004

[47] Nan T, Emori S, Boone C T, Wang X, Oxholm T M, Jones J G, Howe B M, Brown G J, and Sun N X 2015 *Phys. Rev. B* **91** 214416

[48] Khvalkovskiy A V, Cros V, Apalkov D, Nikitin V, Krounbi M, Zvezdin K A, Anane A, Grollier J, and Fert A 2013 *Phys. Rev. B* **87** 020402

[49] Namba T, Tamura K, Hatsuda K, Nakamura T, Ohata C, Katsumoto S, and Haruyama J 2018 *Appl. Phys. Lett.* **113** 053106

[50] Takeuchi Y, Zhang C, Okada A, Sato H, Fukami S, and Ohno H 2018 *Appl. Phys. Lett.* **112** 192408

[51] Ghosh A, Garello K, Avci C O, Gabureac M, and Gambardella P 2017 *Phys. Rev. Appl.* **7** 014004

[52] Mihajlović G, Mosendz O, Wan L, Smith N, Choi Y, Wang Y, and Katine J A 2016 *Appl. Phys. Lett.* **109** 192404

[53] Fukami S, Anekawa T, Zhang C, and Ohno H 2016 *Nat. Nanotechnol.* **11** 621

[54] Cui B, Chen S, Li D, Yun J, Guo X, Wu K, Zhang X, Wang Y, Zuo Y, Gao M, and Xi L 2018 *Appl. Phys. Express* **11** 013001